Proceedings of the ASME 2019
International Mechanical Engineering Congress and Exposition
IMECE2019
November 11-14, 2019, Salt Lake City, UT, USA

IMECE2019-11727

ON CHARACTERIZING UNCERTAINTY SOURCES IN LASER POWDER BED FUSION ADDITIVE MANUFACTURING MODELS

Tesfaye Moges[1]
Mechanical Engineering Department, Indian Institute of Technology Delhi (IITD), New Delhi, India
Engineering Laboratory, National Institute of Standards and Technology (NIST), Gaithersburg, Maryland

Paul Witherell
Engineering Laboratory, National Institute of Standards and Technology (NIST), Gaithersburg, Maryland

Gaurav Ameta
Dakota Consulting Inc.
Silver Spring, Maryland

ABSTRACT

Tremendous effort has been dedicated to computational models and simulations of Additive Manufacturing (AM) processes to better understand process complexities and better realize high-quality parts. However, understanding whether a model is an acceptable representation for a given scenario is a difficult proposition. With metals, the laser powder bed fusion (L-PBF) process involves complex physical phenomena such as powder packing, heat transfer, phase transformation, and fluid flow. Models based on these phenomena will possess different degrees of fidelity as they often rely on assumptions that may neglect or simplify process physics, resulting in uncertainty in their prediction accuracy. Predictive uncertainty and its characterization can vary greatly between models. This paper characterizes sources of L-PBF model uncertainty, including those due to modeling assumptions (model form uncertainty), numerical approximation (numerical uncertainty), and model input parameters (input parameter uncertainty) for low and high-fidelity models. The characterization of input uncertainty in terms of probability density function (PDF) and its propagation through L-PBF models, is discussed in detail. The systematic representation of such uncertainty sources is achieved by leveraging the Web Ontology Language (OWL) to capture relevant knowledge used for interoperability and reusability. The topology and mapping of the uncertainty sources establish fundamental requirements for measuring model fidelity and guiding the selection of a model suitable for its intended purpose.

Keywords: Additive Manufacturing, laser powder bed fusion, uncertainty, ontology

1. INTRODUCTION

Additive manufacturing (AM) produces parts by depositing material layer-by-layer without the requirement of specific tooling based on a 3D model [1]. The laser powder bed fusion (L-PBF) process is the most prominent AM technology capable of producing metallic parts with complex geometry and internal structures [2]. It offers the ability to manipulate the part properties by locally controlling the microstructure and mechanical properties to produce finished parts [3]. The process involves different physical activities such as powder layer formation, laser-powder particles interaction, melt pool formation, and solidification. The fundamental physical phenomena that govern the L-PBF process are powder packing, heat transfer, fluid flow, grain growth, and residual stress formation. Due to the complexity of the physical phenomena and process variabilities, the fusion of powder particles affects mechanical properties, surface finish, and fatigue life of the final parts [4].

There are various parameters in the L-PBF process that potentially affect the quality of the part, as well as the energy and material consumption. Some of these parameters include powder size, powder shape, powder size distribution, laser power, spot size, beam profile, layer thickness, scan speed, hatch distance, build orientation, and pre-heat temperature [5]. To insure part quality and ultimately realize the full potential of the L-PBF process, it is crucial to (a) understand the process complexities, (b) identify the sources of process variability, (c) investigate the effect of process parameters, and (d) determine the optimal process parameters. To achieve these goals, intensive experiment-based studies can be time consuming and costly. Thus, efforts have been devoted to computational models and simulations to investigate the parameter-process-structure-property-performance relationships that lead to part quality improvement [6,7]. Although computational models and simulations are beginning to provide a vast resource for predictive models on which design and process decisions can be made, understanding whether or not a model is an acceptable representation for a given scenario is a difficult proposition.

[1] Corresponding author: tesfaye.moges@nist.gov, tesfaye_mom@yahoo.com

Models based on different physical phenomena of the L-PBF process will possess different degrees of fidelity as they often rely on assumptions that may neglect or simplify process physics, resulting in uncertainty in their prediction accuracy. Predictive uncertainty and its characterization can vary greatly between models. For instance, depending on the (a) type of model, such as a physics-based model or an empirical model, or (b) different measurement techniques, such as optical measurements or thermal measurements. Despite these differences, each source of uncertainty can be related back to the fundamental characteristics of the process. Therefore, it is important to investigate and characterize the potential sources of uncertainty in L-PBF models.

Previous work investigated model fidelity, explored assumptions and approximations of various models, and how this information may be captured [5]. Further work investigated specific sources of uncertainty in L-PBF processes, including a thorough review [8]. In this paper, we build on and harmonize the previous works. We characterize sources of L-PBF model uncertainty, including those due to modeling assumptions (*model form uncertainty*), numerical approximation (*numerical uncertainty*), and model input parameters (*parameter uncertainty*) for low and high-fidelity models. First, the L-PBF models are characterized based on their assumptions by capturing the considered and neglected phenomena and input parameters and output quantities of interest (QoIs). These models include the Rosenthal-based thermal models, the finite element method (FEM)-based continuum thermal models, and the powder-scale thermal-fluid flow models [8]. Following this, characterization of the sources of uncertainty is discussed in detail. Model form uncertainty is characterized based on modeling assumptions by capturing the included and neglected physical phenomena during abstraction and formulation of the model. This uncertainty is commonly quantified using a validation metric by comparing simulation results against measurement data. Numerical uncertainty arises primarily from discretization error and is characterized using code and solution verification. Model input parameter uncertainty comes from the inherent variability present in input parameters or those parameters whose exact values are not known and cannot be directly measured. Then, the characterization of models and uncertainty sources is represented using an ontology to capture relevant knowledge that can be used for interpretability and reusability.

The organization of the paper is as follows. We first briefly present the state-of-the-art on uncertainty related studies for L-PBF process in Section 2. We then discuss the characterization of L-PBF models focusing on their assumptions by capturing the considered and neglected phenomena in Section 3. Then, in Section 4, we present the investigation and characterization of L-PBF uncertainty sources. A case study to illustrate the characterization approach is presented in Section 5. The systematic representation of models and uncertainty sources is described in Section 6. We view this work to be an essential step to establish fundamental requirements for measuring model fidelity, and for guiding the selection of a model suitable for its intended purpose.

2. BACKGROUND

It has been highlighted that computational models and simulations play significant roles in understanding the AM process phenomena and predicting optimum process parameters and hence are important contributing factors to achieving desired part performance and reducing the numbers of faulty parts [4,9]. There has been tremendous effort to develop computational thermal models to understand the thermal history and predict melt pool geometries in L-PBF process. These models can be broadly categorized into three groups: the Rosenthal-based thermal models, the FEM-based thermal models, and the powder-scale thermal-fluid flow models. The Rosenthal-based thermal models analytically solve the heat conduction equation for a moving heat source [10]. The only heat transfer mechanism considered in these models is thermal conduction; those due to convection and radiation are neglected. The models provide low fidelity predictive results, but they are computationally efficient. However, the heat transfer phenomena and phase transformations that exist in the L-PBF process are complex and hence the governing heat transfer equations and boundary conditions that capture these phenomena are difficult to solve analytically. Thus, to understand the thermal history in detail and accurately predict the temperature fields and melt pool characteristics, various numerical models have been developed [8].

The FEM-based thermal models solve the heat transfer governing equations by discretizing the spatial domain into a finite number of elements and the temporal transient phenomena into time steps regardless of geometrical complexity. In these models, the powder bed is considered as a continuum block of material with effective thermo-physical properties, and the heat transfer mechanisms and distribution of absorbed energy are accounted for. However, the phenomena related to melt pool flow are neglected. To understand the fluid flow of the molten pool, more realistic numerical models based on powder-scale, thermal-fluid flow have been developed [11]. These models represent the L-PBF process more realistically by directly accounting for the phenomena related to powder packing (powder size, shape, and size distribution) and melt pool flow (surface tension, shrinkage, recoil pressure, and others). In addition to the common process signatures (temperature fields and melt pool geometries), these models can be used to investigate the formation of different defects such as balling, porosity, and delamination between layers and substrate. The critical challenge of these models is that they are computationally expensive and thus infeasible to use for full part-scale simulations and studying parameter optimizations as these problems require a large number of simulations.

Though experimental-based uncertainty analysis can provide the actual variabilities present in AM processes [12,13], this approach is time consuming and costly. To deploy computational models for design and process decision making and ultimately for part qualification, their degree of fidelity needs to be known first. Thus, understanding the sources of uncertainty is necessary to determine the degree of model fidelity and conduct uncertainty management to identify the main sources of error.

The uncertainty related studies in L-PBF models are relatively new and have started receiving increasing attention in recent years in the AM community [8,14–16]. Some of these studies are reviewed as follows. Moser et al [17] and Ma et al [18] identified the critical input parameters that largely influence the predictive accuracy of the FEM-based thermal model by assigning a probability density function (PDF) to account for parameter variability using a stochastic collocation approach and fractional factorial design of experiment (DOE), respectively. Nath et al [19] conducted uncertainty analysis on the FEM-based thermal model by constructing a statistical surrogate model using a Gaussian process to replace the computationally expensive physics-based thermal model. They also extended the uncertainty analysis to a solidification model to quantify the uncertainty in grain size distribution of microstructure. Kamath [20] conducted uncertainty analysis on the Eagar-Tsai Rosenthal-based thermal model [21] that considers Gaussian-distributed heat source and powder-based thermal model that was developed by Verhaeghe et al [22] using a regression tree and Gaussian process surrogate models. Tapia et al. [23] used polynomial chaos expansions for uncertainty propagation analysis in the Eagar-Tsai Rosenthal-based thermal model and the FEM-based thermal model. Tapia et al. [24] used a Gaussian process surrogate model for the powder-scale thermal-fluid flow model which was developed by Khairallah et al. [25]. Yang et al. [26] investigated different surrogate modeling techniques and discussed the implementation of adaptive sampling method to manage the sources of uncertainty in AM predictive models. There are some research efforts that use deep learning for classification of melt pool size [27] and machine learning for a data-driven continuous construction of AM knowledge [28]. A thorough literature review on machine learning applications in AM can be found in Razvi et al. [29].

The stated previous works are primarily focused on uncertainty analysis related to input parameters to identify the most critical parameters that influence the output QoIs. However, to fully understand the fidelity of a model and perform uncertainty analysis, it is important to investigate all sources of uncertainty: those due to modeling assumptions, numerical approximations, input parameters, and uncertainty due to measurement errors for model validation. Lopez et al [16] made an effort to identify these sources of uncertainty for the Rosenthal-based thermal model considering melt pool width as an output QoI. To quantify uncertainty propagation of input parameters, the Monte Carlo simulation was directly imposed on the physics-based model as the model is computationally efficient. Moges et al [15] extended this work to further investigate and quantify all sources of uncertainty for the Rosenthal-based as well as for the FEM-based thermal models to predict melt pool width. A fractional factorial DOE was used to drive a statistical response surface model on which the Monte Carlo simulation was imposed to quantify parameter uncertainty. Other uncertainty related studies for L-PBF models can also be found in Hu and Mahadevan [30], Mahmoudi et al [31], and Ghosh et al [32]. In present study, we characterize these uncertainty sources and represent them in a systematic fashion to capture their effects on predictive accuracy of computational models.

3. THE L-PBF THERMAL MODELS

The investigation and characterization of sources of uncertainty in computational models begin from understanding the assumptions, abstractions, and governing equations on which these models rely and capturing the included and neglected physical phenomena. Thus, it is important to first characterize the existing thermal models based on their assumptions as it also provides conceptual understanding of model fidelity [5]. In this section, the characterization of thermal models based on their assumptions, governing equations, and included and neglected physical phenomena along with input parameters and output QoIs is briefly presented. Although there are a wide variety of boundary conditions, material models, and methods associated to the models, our focus is on the general description of the L-PBF thermal models.

3.1 The Rosenthal-based thermal models

The conduction mode of heat transfer is the main governing phenomenon in laser-powder interaction in L-PBF process. The heat conduction equation for a moving heat source is expressed in Equation (1) [33].

$$\rho C_p \frac{\partial T}{\partial t} = (\nabla \cdot k \nabla T) + Q, \tag{1}$$

where ρ is density, C_p is specific heat capacity, k is thermal conductivity, and Q is internal heat. Assuming the heat source distribution as a point or Gaussian heat source moving in the x direction on a surface of a semi-infinite space, Rosenthal [10] and Eagar and Tsai [21] determined the temperature T at a given time t, respectively. The Rosenthal-based thermal models can be used as a foundation to build more realistic approaches by considering the different laser beam distributions (line, cylindrical, Gaussian, or ellipsoid) [33]. The characterization of these models in terms of input parameters, outputs, assumptions, and considered and neglected phenomena is given in Table 1.

Table 1: Characterization of the Rosenthal-based thermal models

Input parameters	Laser power, scan speed, absorption coefficient, melting temperature, thermal conductivity, density, specific heat capacity, latent heat of fusion, preheat temperature
Output QoIs	Temperature fields, cooling rates, and melt pool dimensions (width and length)
Assumptions	Surface energy distribution, heat source distribution (point, cylindrical, ellipsoid, or Gaussian), continuum material
Considered phenomena	Energy absorptivity, absorbed energy distribution (only cross-section), moving heat source (scan speed), thermal conduction, latent heat of fusion
Neglected phenomena	Absorbed energy distribution (penetration), heat convection, surface radiation, latent heat of vaporization, all phenomena related to melt pool flow, phase transformation, powder particle packing

3.2 The FEM-based thermal models

To capture the steep thermal gradients near the laser spot and heat affected zone and transient nature of the heat transfer phenomena, the FEM-based thermal models are commonly used in L-PBF process [34]. In FEM models, the layer of powder particles is assumed as a continuum block of material with effective thermo-physical properties. The continuum powder bed is discretized into finite elements and the governing heat conduction equation is solved locally with initial condition and boundary conditions. To solve Equation (1) numerically, the initial condition assumed a uniform preheat temperature throughout the powder bed at time $t = 0$ and the boundary conditions on the top surface are given using Equation (2) [34].

$$-k\nabla T \cdot \boldsymbol{n} = q + h(T - T_0) + \varepsilon\sigma(T^4 - T_0^4), \tag{2}$$

where $\boldsymbol{n}$ is the vector normal to the surface, q is thermal heat flux, h is convection coefficient, ε is thermal radiation coefficient, T_0 is preheat temperature, and σ is Stefan-Boltzmann constant. The surface heat flux of the laser beam is given using Equation (3) assuming Gaussian heat source distribution [35].

$$q = \frac{2AP}{\pi r_b^2} \exp\left(\frac{-2r^2}{r_b^2}\right), \tag{3}$$

where A is absorption coefficient, P is laser power, r_b is laser spot radius, and r is radial distance.

Similarly, the characterization of the FEM-based thermal models in terms of input parameters, outputs, assumptions, and considered and neglected phenomena is summarized in Table 2.

Table 2: Characterization of the FEM-based thermal models

Input parameters	Laser power, scan speed, absorption coefficient, latent heat of fusion, solidus temperature, liquidus temperature, thermal conductivity, density, specific heat capacity, preheat temperature, layer thickness, beam radius, emissivity, convection coefficient
Output QoIs	Temperature field, cooling rates, melt pool dimensions (width, depth, and length) and shape
Assumptions	heat source distribution (line, double ellipsoid, or Gaussian), continuum powder bed
Considered phenomena	Energy absorptivity, moving heat source (scan speed), absorbed energy distribution (cross section and penetration), thermal conduction, heat convection, surface radiation, latent heat of fusion
Neglected phenomena	Latent heat of vaporization, all phenomena related to melt pool flow (surface tension, Marangoni effect, etc.), phase transformation, powder particle packing (powder size distribution, powder particle contact forces)

3.3 The powder-scale thermal-fluid flow models

Further understanding of the L-PBF process can be achieved by accounting for the actual physics of the process. As stated above, these include considering the powder bed as distributed powder particles instead of a continuum block of matter and incorporating the effect of melt pool flow as well as the gas-liquid-solid interactions. Powder-scale thermal-fluid flow models are able to consider these physical phenomena and simulate the L-PBF process. In these models, different physical phenomena that potentially govern the fusion process and part quality can be captured. To simulate these physical phenomena, the 3D transient conservation equations of mass continuity, momentum, and energy are solved numerically. The conservation equations are expressed using Equations (4)-(6) [36].

$$\nabla \cdot (\rho \vec{v}) = 0\,, \tag{4}$$

$$\frac{\partial}{\partial t}(\rho \vec{v}) + \nabla \cdot (\rho \vec{v} \otimes \vec{v}) = \nabla \cdot (\mu \nabla \vec{v}) - \nabla \mathrm{p} + \rho \vec{\mathrm{g}} + F_b, \tag{5}$$

$$\frac{\partial}{\partial t}(\rho h) + \nabla \cdot (\rho \vec{v} h) = q + \nabla \cdot (k \nabla T), \tag{6}$$

where $\vec{v}$ is velocity vector, μ is viscosity, p is pressure, $\vec{\mathrm{g}}$ is gravitational acceleration vector, F_b is buoyancy force, h is enthalpy, and $\otimes$ is the Kronecker product. The position of the free surface in terms of phase fraction (F) at the void-liquid interface as a function of time is tracked using the volume of fluid (VOF) method and it is expressed in Equation (7) [37].

$$\frac{\partial F}{\partial t} + \nabla \cdot (\vec{v} F) = 0, \tag{7}$$

The Equations (4) to (7) are solved together to provide the 3D transient temperature and velocity fields using boundary conditions such as the heat exchange between the top surface and the surroundings and the Marangoni shear stress induced by the special variation of surface tension which are expressed using Equations (8) and (9) [37].

$$-k\nabla T \cdot \boldsymbol{n} = h(T - T_0) + \varepsilon\sigma(T^4 - T_0^4) + q_{evap}, \tag{8}$$

$$\gamma(T) = \gamma_m + \frac{d\gamma}{dT}(T - T_m), \tag{9}$$

where q_{evap} is evaporation heat loss, γ is the surface tension at the surface temperature T, γ_m is the surface tension at the melting temperature, and $\frac{d\gamma}{dT}$ is the temperature coefficient of surface tension.

In addition to the convective and radiative heat loss from the top free surface, under intense laser irradiation, heat loss due to evaporation and the resulting recoil pressure need to be considered [37]. To predict the amount of energy absorbed by the powder bed, a 3D volumetric heat source that accounts for multiple reflections of the laser beam inside the powder layers has to be considered [7]. Moreover, the temperature dependent material properties of the powder material significantly affect the accuracy of the L-PBF models. Since the powder bed consists of powder particles as well as shielding gas within the interparticle space, the effective temperature dependent properties, such as density, specific heat, and thermal conductivity of the powder bed depend on properties of the powder material and shielding gas [38]. The packing structure of the powder bed in terms of packing density plays a crucial role in simulating the L-PBF process and needs to be coupled with the thermal-fluid flow models. The choice of powder particle distribution (Gaussian, bimodal, uniform, or mono-sized) significantly influences the packing structure of the powder bed in terms of packing density and porosity. The powder bed models are predominantly characterized by particle shape and size, particle size distribution

Table 3: Characterization of powder-scale thermal-fluid flow models

Input parameters	Laser power, scan speed, absorption coefficient, latent heat of fusion, solidus temperature, liquidus temperature, boiling temperature, thermal conductivity, density, specific heat capacity, ambient temperature, layer thickness, beam radius, emissivity, convection coefficient, surface tension coefficient, viscosity, latent heat of evaporation
Output QoIs	3D transient temperature fields and velocity distributions, melt pool dimensions (width, depth, and length), melt pool shape, surface roughness, geometric dimension, porosity, voids
Assumptions	heat source (Gaussian or double ellipsoid), Newtonian flow and incompressible molten metal
Considered phenomena	Energy absorptivity, absorbed energy distribution (cross section and penetration), multiple reflections effect, thermal conduction, heat convection, surface radiation, latent heat of fusion and evaporation, melt pool flow (surface tension, Marangoni effect, buoyancy, gravity, recoil pressure, mass change due to evaporation and condensation), phase transformation (melting, solidification, vaporization, condensation), powder particle packing (powder size distribution, powder particle contact forces: collision, friction, adhesion)
Neglected phenomena	Mass change due to chemical reaction (oxidation), solid-state phase transformation, gas flow and interaction with solid and liquid, chemical element diffusion and chemical reaction

packing density, layer thickness, and re-coater velocity and geometry [8]. The heat transfer-fluid flow models can also be coupled with the solidification and residual stress and distortion models to determine microstructure and solidification parameters and mechanical properties of the fabricated parts [39]. The characterization of the powder-scale thermal-fluid flow models in terms of input parameters, outputs, assumptions, and considered and neglected phenomena is summarized in Table 3.

4. CHARACTERIZING L-PBF UNCERTAINTY SOURCES

The beginning of verification, validation, and uncertainty quantification (V&V UQ) for any scientific computing is to identify and characterize the sources of uncertainty [40]. The flow of uncertainty sources and the verification and validation and UQ adapted from Assouroko et al [5], Lopez et al [16], and ASME V&V-20 Standard [41] for L-PBF computational models is depicted in Figure 1. Using the basic principles of physical laws, such as conservation of mass, momentum, and energy, mathematical models are abstracted and formulated based on assumptions to represent the L-PBF physical process. Such assumptions during mathematical model development cause model form uncertainty that results in inaccurate prediction of output QoIs. To solve the partial differential equations and simulate the L-PBF physical phenomena, computational models use numerical approximations. Such approximations cause numerical uncertainty that undermines the predictive accuracy of the models. The V&V UQ process involves verification that verifies whether the computational model accurately solves the mathematical equations and quantifies the numerical uncertainty due to discretization errors. The validation process evaluates how accurately the computational model represents the L-PBF physical process and estimates the model bias and model form uncertainty by comparing measurement results along with associated uncertainty against simulation results along with numerical and parameter uncertainties. The parameter uncertainty of an output QoI is estimated by propagating uncertainties of input parameters through computational model or surrogate model (if the model is computationally expensive). This section discusses the characterization of these sources of uncertainty through V&V UQ approaches.

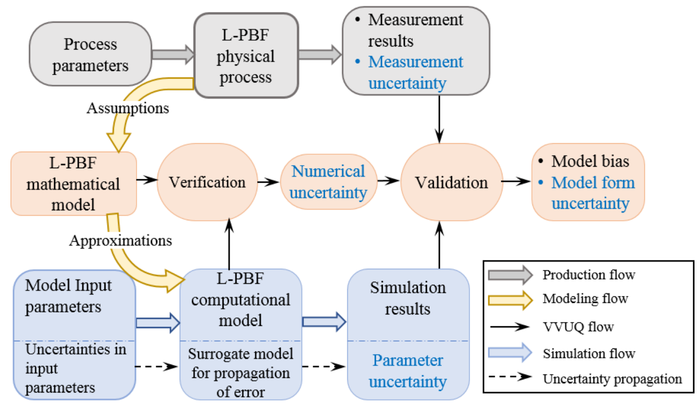

FIGURE 1: UNCERTAINTY SOURCES AND V&V UQ IN L-PBF COMPUTATIONAL MODELS

4.1 Model form uncertainty

The mathematical models only capture certain physical phenomena of the L-PBF process as they are abstracted and formulated based on assumptions and simplifications, and hence they cannot exactly represent the physical mechanisms of the process. As discussed in Section 3, there is a wide range of L-PBF thermal models ranging from low to high fidelity and models within the same level of fidelity. The predictive accuracy of these models potentially depends on the assumptions, considered, and neglected process physics (Tables 1-3). Model form uncertainty arises due to assumptions associated with physical phenomena that neglect or simplify some physics of the process. The predictive accuracy of models across different fidelity or within the same level of fidelity is different due to model form uncertainty. For instance, the assumptions and simplifications of physical phenomena associated with boundary conditions and temperature dependent properties in modeling of heat transfer and phase transformations can lead to inaccurate prediction of temperature gradient and melt pool geometry [8]. The assumptions associated with the distribution of heat source as a point, line, or double ellipsoid heat source significantly conflict with the measured power density distribution. Moreover, ignoring the convective heat transfer, which is one of the main mechanism of heat transfer within the melt pool, can lead to highly inaccurate temperature fields and cooling rates [7].

Model form uncertainty is commonly characterized using a validation approach that evaluates the predictive accuracy of a model by comparing simulation results against measurement results collected under the same condition [42]. Since uncertainties associated with model input parameters propagate through the model and potentially affect the accuracy of simulation results, the values of these parameters need to be first measured and their uncertainties need be characterized. Second, the measurement results along with their uncertainties need to be obtained to perform an effective validation process and estimate model form uncertainty. The ASME V&V 20 Standard for Verification and Validation in Computational Fluid Dynamics and Heat Transfer [41] discussed the verification and validation activities, along with quantifying sources of uncertainty, in heat transfer and computational fluid dynamics. Since L-PBF process involves heat transfer and melt pool flow phenomena, this standard can be suitable for characterizing sources of uncertainty in L-PBF models. The interval within which model bias falls is characterized by validation metrics and expressed using the following expression (10).

$$\delta_{model} \in [E - u_{val}, E + u_{val}], \tag{10}$$

where E is the comparison error between simulation result and measurement result and u_{val} is validation uncertainty. The validation uncertainty that accounts for the sources of uncertainty due to model input parameters (u_{input}), numerical approximations (u_{num}), and measurement errors (u_D) is evaluated using Equation (11). Therefore, all sources of uncertainty need to be characterized for proper assessment of predictive accuracy of L-PBF models.

$$u_{val} = \sqrt{u_{num}^2 + u_{input}^2 + u_D^2}, \tag{11}$$

4.2 Numerical uncertainty

The governing mathematical equations that capture the complex L-PBF physical phenomena are difficult to solve analytically. Thus, numerical methods are often used to solve these equations based on simplification and approximation to obtain approximate solutions. This approximation introduces numerical uncertainty into the predicted QoIs. There are different sources of uncertainty associated with numerical approximations in any computational simulations, such as truncation error, discretization error, error due to computer programming mistakes, iteration error, and round-off error [43]. Among these sources of uncertainty, discretization error is often considered as the main source of uncertainty due to its larger magnitude and it has been the center of attention in most verification related studies [43]. The verification process insures that a numerical model accurately represents the underlying mathematical equations and estimates numerical uncertainty due to discretization errors. Thus, numerical uncertainty associated with numerical approximations is characterized by the model verification process. To address this matter, verification is divided into two fundamental parts: code and solution verifications [44].

Code verification makes sure that an algorithm or a computer code is free of mistakes or bugs. This is achieved using software quality assurance (SQA) techniques or the method of manufactured solutions (MMS) by comparing predictive outputs with analytical solutions or manufactured solutions if analytical solutions are difficult to compute [43]. In L-PBF models, different simulation codes have been used to numerically estimate the output QoIs. These include discrete element method (DEM) codes to determine powder packing density, OpenFOAM, Flow-3D, or ALE3D code to simulate heat transfer and fluid flow as well as other commercial codes and softwares like ANSYS and ABAQUS to predict the QoIs in heat transfer and residual stress analyses [8]. The Rosenthal-based analytical solution of temperature field is commonly utilized to conduct code verification for L-PBF thermal models. Hence, code verification needs to be conducted to make sure that these codes have satisfied the order of accuracy test.

Solution verification estimates the sources of uncertainty associated with numerical approximations. The governing partial differential equations are solved by discretizing the spatial domain of interest into a finite number of elements and the time advancement into a finite time step. This approach is common in L-PBF models that use different numerical methods, such as FEM, FDM, FVM, DEM, LBM, and CFD [8]. This discretization causes numerical uncertainty in computational simulations. There are different techniques to quantify this source of uncertainty, such as Richardson extrapolation, Roache's grid convergence index, and others [43]. Discretization error is commonly estimated by first computing predictive outputs determined at different grids with course, medium and fine mesh sizes. Roache [45] used grid convergence index (GCI) to convert the discretization error determined from Richardson extrapolation into uncertainty, and the equations used to compute numerical uncertainty are given in Equations (12)-(14). A detailed explanation and formulation on code and solution verifications taking heat transfer and computational fluid dynamics models as a case study can be found in ASME V&V 20 Standard [41] and Roy and Oberkampf [43]. Since numerical-based L-PBF models are computationally expensive, statistically-driven surrogate models are commonly developed to overcome this issue. This introduces surrogate model uncertainty due to the limited number of training and testing data.

$$GCI = F_s \frac{\epsilon_{ext}}{r_{21}^p - 1}, \tag{12}$$

$$\epsilon_{ext} = \left|\frac{f_{\text{ext}} - f_1}{f_{\text{ext}}}\right|, f_{\text{ext}} = \frac{r_{21}^p f_1 - f_2}{r_{21}^p - 1}, p = \frac{\ln(|f_3 - f_2|/|f_2 - f_1|) + q(p)}{ln r_{21}}, \tag{13}$$

$$\begin{gathered} q(p) = ln\left[\left(r_{21}^p - s\right)/\left(r_{32}^p - s\right)\right], \\ s = sign[(f_3 - f_2)/(f_2 - f_1)], \end{gathered} \tag{14}$$

where GCI is grid convergence index, F_s is factor of safety, f_1, f_2, and f_3 are simulation results at course h_1, medium h_2, and fine h_3 mesh sizes, r_{21} and r_{32} are the mesh refinement ratios, p is order of convergence. For a constant mesh refinement ratio, $q(p) = 0$. Otherwise, the order of convergence is computed recursively with initial guess $q(p) = 0$. A numerical uncertainty is computed by multiplying the GCI with a simulation result.

4.3 Parameter uncertainty

Computational models utilize different input parameters to simulate the behavior of physical phenomena existing in L-PBF process. There is inherent variation in process parameters and in some cases, precise values of some parameters are not known due to imprecise measurement methods or inaccurate estimation of physical properties as the L-PBF process exhibits phase transformation at a small length scale within a very short period of time. Thus, the sources of parameter uncertainty come from natural variability existing in process parameters and/or due to parameters whose exact values are not known or cannot be directly measured. For instance, temperature dependent material properties possess uncertainty due to (a) difficulty in accurately measuring their values especially at high temperature, (b) availability and usage of different measuring techniques, or (c) different values reported in the literature [8]. As a result, any uncertainty associated with input parameters propagates into simulation output QoIs through computational models and results in reduction of predictive accuracy. Depending on the amount of information known regarding the distributions of parameter uncertainty, the model input parameter uncertainty can be commonly classified into two categories: aleatory and epistemic uncertainty [14].

Aleatory uncertainty is described as the uncertainty that arises due to natural variation or randomness in a system. There are a significant number of sources of parameter uncertainty in L-PBF process that fall under this category. These include uncertainty sources due to variation in powder size, shape, and size distribution, fluctuations and inherent drift in laser system and galvanometer, vibration in motion and position of built platform and re-coater arm that alter layer thickness, and others. The uncertainty sources that cause variation in process parameters, temperature dependent properties, and absorption coefficient are discussed in Moges et al [8]. This type of uncertainty is characterized by a distribution function, either a probability density function (PDF) or a cumulative distribution function (CDF) to represent the frequency of occurrence [42]. To define the distribution of parameter uncertainty, enough data/knowledge is required.

Epistemic uncertainty is a type of uncertainty that arises due to lack of knowledge and thus it can be reduced by introducing additional information. If a distribution function is assumed for input parameter uncertainty without having enough information, it introduces additional uncertainty into output QoIs. Such an assumption is common in L-PBF input parameters due to the limited number of samples to precisely define the form and parameters of the distribution function. For example, there is limited and sparse data of absorption coefficient and coefficient of friction parameters to accurately define the type and parameters of distribution functions. This uncertainty is commonly characterized by a distribution function to represent the degree of belief [42].

There are different approaches to propagate sources of parameter uncertainty through a model and quantify uncertainty of output QoIs. These include Monte Carlo sampling, response surface methods, stochastic collocation method, polynomial chaos expansion, Gaussian process model, support vector machines, and others [42,46]. For instance, Monte Carlo sampling randomly select a number between zero and one and applies a distribution function to obtain the corresponding parameter sample. This method requires a large number of simulations and hence is only applicable for models that are computationally efficient. For intensive simulation models, the common approach for propagating input parameter uncertainty sources is through surrogate models, such as polynomial chaos expansion, Gaussian process, and others. For example, polynomial chaos expansion expresses output QoI in terms of model input parameters along with their uncertainties using orthogonal basis functions and coefficients and the general expression is given by Equation (15) [14,23].

$$y(\mathbf{x}) = \sum_{j=0}^{N_b} a_j \psi_j(\mathbf{x}), \tag{15}$$

where $\mathbf{x}$ is set of input variables, $y(\mathbf{x})$ is output response, a_j is coefficient of basis function, $\psi_j(\mathbf{x})$ is orthogonal basis function, and N_b is number of basis functions.

4.4 Measurement uncertainty

To accurately compare simulation results with experimental data and perform a validation process to estimate model form uncertainty, measurement results need to be provided along with associated uncertainty of the output QoIs. Measurement uncertainty originates from imprecise measurement methods and/or error in equipment calibration. Different measurement techniques, such as optical measurements or thermal measurements to conduct in-process monitoring, result in different uncertainty in surface temperature due to the difference in measurement methods [47]. Measurement uncertainty is mainly characterized by different components, such as mean, standard deviation, and probability distribution. These components can be evaluated using statistical method by utilizing the results from a series of measurements. The standard way to evaluate measurement uncertainty from experimental data is described in the "Guide to the Expression of Uncertainty in Measurement (GUM)" [48]. The confident interval of the measurement uncertainty is derived from the standard deviation of a sample population which is evaluated using Equation (16).

$$s = \left[\frac{1}{n-1}\sum_{i=1}^{n}(y_i - \bar{y})^2\right]^{1/2}, \tag{16}$$

where s is standard deviation, n is number of measurements, y_i is measured QoI, and $\bar{y}$ is mean value of all measurement results.

5. CASE STUDY: CHARACTERIZING UNCERTAINTY SOURCES IN L-PBF THERMAL MODEL

In this case study, a Rosenthal-based semi-analytical melt pool model is selected to demonstrate the concept presented in

Section 4. This semi-analytical melt pool model solves the heat conduction equation for a moving heat source (Equation 1) using a set of ordinary differential equations that describes the motion of isotherms on the surface of the powder bed. By assigning one of the isotherms to the melting temperature, the model can be used to predict the melt pool width. This model is first developed for laser cladding using isotherm migration method [49] and adjusted for use in L-PBF process [16]. The method extends the Rosenthal's solution for moving heat source to consider the temperature-dependent material properties. This model is highly simplified thermal model that neglects multiple physical phenomena of the L-PBF (Table 1), it is suitable for quick prediction of melt pool dimensions.

All sources of uncertainty described in Section 4 exist in this semi-analytical melt pool model. Due to the assumptions in terms of point heat source distribution, continuum powder bed, and ignoring melt pool flow phenomena (see Table 1), the model comprises of model form uncertainty associated with these assumptions. The temperature increment used to assign the isotherms on the powder bed surface induces discretization error that causes numerical uncertainty. The uncertainty associated with input parameters propagates through the model and causes uncertainty on the predicted melt pool width. Measurement uncertainty associated with melt pool width is also plays major role in model validation. The detailed analysis and UQ on this regard is given in Moges at al [15].

As discussed in Section 4, estimation of modeling error begins from code and solution verification. It was reported that the code verification for the model used in this case study was conducted using manufactured solution and the method converges to the Rosenthal's analytical solution [16]. The solution verification that estimates numerical uncertainty due to discretization error is conducted using Roache's grid convergence index. The GCI that estimates the 95% convergence is determined using Equation (12) based on the values of melt pool width obtained at course, medium, and fine grid refinements. The estimated melt pool width along with numerical uncertainty at laser power 195 W, scan speed 800 mm/s, and absorption coefficient 0.6 for IN625 material is (127.5 ± 2.3) μm.

The source of uncertainty due to unknown input parameters is quantified using full factorial design of experiment (DOE) analysis assuming normal distribution for the parameters given in Table 4. A statistically-driven surface response that uses to estimate parameter uncertainty of the melt pool width is first derived from DOE analysis. Then Monte Carlo simulation is conducted to determine the probability distribution of melt pool width. The histogram of the melt pool widths for 10,000 samples and fitted normal distribution is shown in Figure 2. The average of the predicted melt pool widths and the parameter uncertainty that represents the 95% confidence interval is obtained to be (138.7 ± 12.8) μm.

Table 4: Input parameters for uncertainty propagation

Input parameters	Nominal value	% variation
Laser power	195 W	2.5%
Scan speed	800 mm/s	1.5%
Absorption Coefficient	0.6	20%
Heat capacity	$c_p(T)\ J/kgK$	3%
Thermal conductivity	$k(T)\ W/mK$	3%

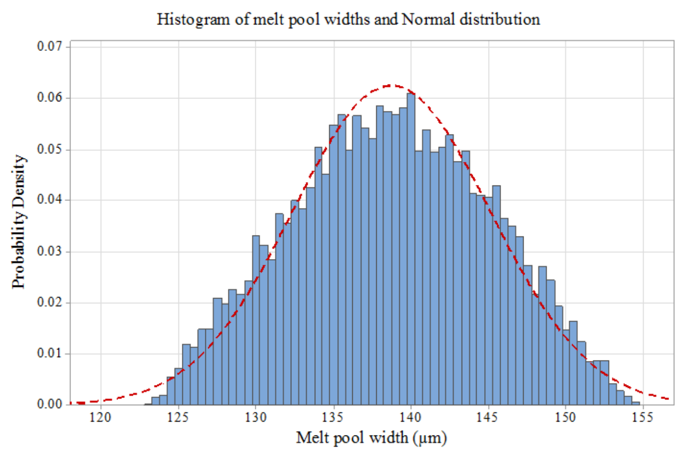

FIGURE 2: PROBABILITY DENSITY OF PREDICTED MELT POOL WIDTHS

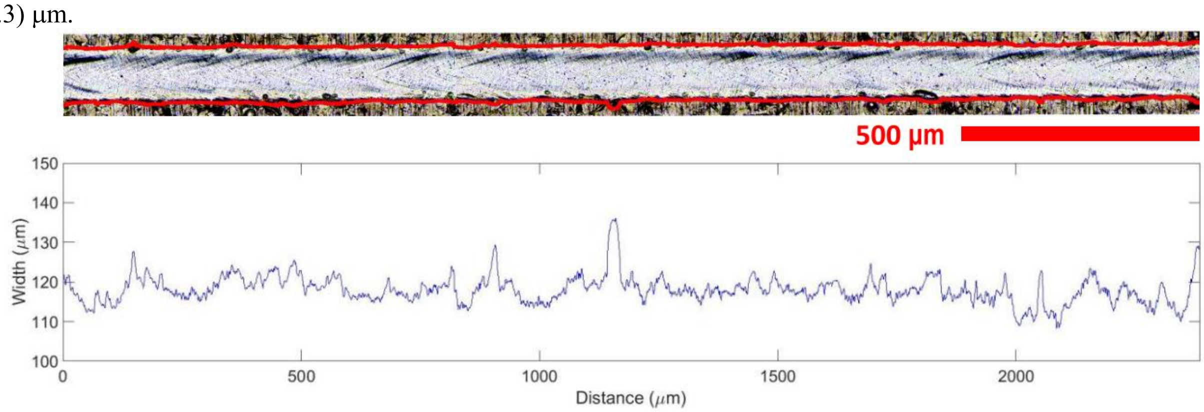

FIGURE 3: MEASUREMENT OF MELT POOL WIDTH FROM OPTICAL IMAGE OF SCAN TRACK. FIGURE ADOPTED FROM FOX ET AL. [50]

To determine measurement uncertainty for model validation and estimate model uncertainty, melt pool width was measured from the image of scan track taken using optical microscope by manually tracing the edges of the scan track and using a software to determine the distance between the traces as shown in Figure 3 [50]. The measured melt pool average and standard deviation IN625 material at 195 W laser power and 800 mm/s scan speed are 132.2 μm and 14.1 μm, respectively. Thus, the 95% confidence interval is ± 28.2 μm. In addition, manually tracing the edges of the track induces ± 2 μm uncertainty.

The validation uncertainty, assuming all uncertainty sources are independent, is determined using Equation (11) and is estimated to be (127.5 ± 32.9) μm. The comparison between the predicted and measured melt pool width and the confidence interval obtained from validation uncertainty is depicted in Figure 4.

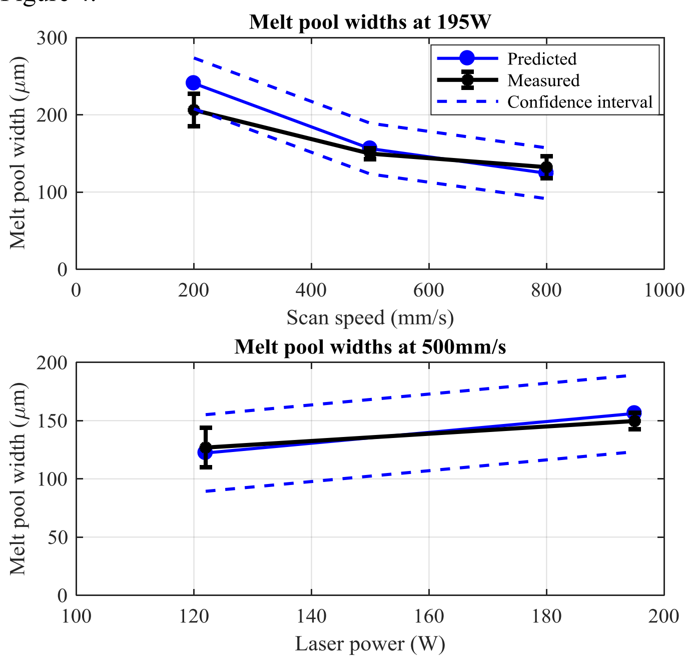

FIGURE 4: PREDICTED AND MEASURED MELT POOL WIDTH AND 95% CONFIDENCE INTERVAL

6. REPRESENTATION OF L-PBF MODELS AND UNCERTAINTY SOURCES

To capture relevant knowledge of the L-PBF models and sources of uncertainty, systematic representation of their characterization is essential. For this purpose, the Web Ontology Language (OWL)-based ontology is leveraged to extract relevant knowledge that can be useful for interoperability and reusability. There are some research efforts that use ontology-based knowledge representation in AM [5,51,52]. This section presents the addition of specific classes and attributes into our previous AM ontology [5] in order to capture knowledge associated to particle-scale thermal-fluid flow models and sources of uncertainty. First, we discuss the representation of the L-PBF models focusing on the powder particle-based models, and then we present the representation of uncertainty sources focusing on their classifications and their relationships with the models.

6.1 Representation of L-PBF models

The proposed ontology in the present study captures the formulations, assumptions, input parameters, output QoIs, and predictive models of the five main physical mechanisms of the L-PBF process: powder layer deposition, heat source-powder interaction, melt pool formation, solidification and grain growth, and the occurrence of residual stress and distortion formation. The main class named *LPBFModel* comprises of the following subclasses: *Formulation*, *Assumption*, *InputParameters*, and *Prediction,* with prefix of *LPBFModel,* as well as *LPBFPredictiveModel*. The *LPBFModelFormulation* subclass involves the mathematical formulations used to capture the aforementioned physical mechanisms of the L-PBF process. For instance, the *MeltPoolModelFormulation* includes the conservation equations of mass, momentum, and energy that capture the heat transfer and fluid flow phenomena in the melt pool. The modeling assumptions and simplifications used while formulating the physical phenomena are captured under the subclass called *LPBFModelAssumption*. For example, this subclass captures the assumptions associated to distribution of heat source: point, cylindrical, ellipsoidal, or Gaussian; powder bed material distribution: continuum or distributed powder particle; powder size distribution: mono-size, bi-modal, uniform, Gaussian, or positively skewed. The subclass that captures the input parameters including process parameters: laser power, scan speed, layer thickness, beam size, etc. and material properties: thermal conductivity, density, heat capacity, melting temperature, etc., is *LPBFModelInputParameter*.

The output QoIs of the L-PBF predictive models are captured by the *LPBFModelPrediction* subclass. This involves the outputs of (a) powder bed model: packing density, coordination number, and radial distribution function; (b) heat source model: absorbed energy, absorbed energy distribution, and effective absorption coefficient; (c) melt pool model: temperature gradient, melt pool dimensions: width, depth, and length, defects: balling, keyhole, and layer delamination, and porosity: gas pores and inter-track voids; (d) solidification model: grain size, grain morphology, and grain orientation; (e) residual stress and distortion model: residual stress and strain distribution, deformation history, fatigue life, and shrinkage. The last subclass under *LPBFModel* is *LPBFPredictiveModel* and this captures the different predictive models in L-PBF process. These models include (1) powder bed models: raindrop method and discrete element method (DEM); (2) heat source model: Beer Lambert, ray tracing, radiation transfer, and surface heat flux; (3) melt pool models: Rosenthal-based model, FEM thermal model, CFD-based model, and lattice Boltzmann method; (4) solidification model: phase field method and cellular automata; (5) residual stress and distortion model: thermomechanical FEM-based model and simplified mathematical model.

6.2 Representation of L-PBF uncertainty sources

The uncertainty related aspects of the L-PBF models, which include sources of uncertainty, uncertainty quantification approaches, and types of uncertainty, are captured in the proposed ontology. The *LPBFUncertainty* class involves subclasses such as *TypeOfUncertainty*, *LPBFUncertaintySource*, and *LPBFUQMethod*. As discussed in previous section, the *TypeOfUncertainty* in any scientific computing can be categorized as *AleatoryUncertainty*, *EpistemicUncertainty*, or *CombinedUncertainty*. As mention in previous section, aleatory uncertainty is due to natural randomness of input quantities or perturbation in a system and cannot be reduced. There are different uncertainty sources that fall under this category. These include variation in measurement results, inherent drift in laser supply system, fluctuation in laser power, scan speed, and beam radius, variation in powder size, shape, and size distribution, friction coefficient, and absorption coefficient of a powder bed. On the other hand, epistemic uncertainty comes from lack of knowledge and can be reduced by introducing more information. The L-PBF uncertainty sources that fall under this category include uncertainty due to modeling assumptions that neglect some physical phenomena (model form uncertainty), uncertainty due to numerical approximation (numerical uncertainty), limited measurement data, error in instrument calibration, imprecise measurement method, and uncertainty in distribution type and parameters due to sparse data.

The *LPBFUQMethod* represents different methods and standard approaches to quantify model form, numerical, parameter, and measurement uncertainties. For instance, measurement uncertainty can be quantified using a standard approach GUM, numerical uncertainty by verification approach, model form uncertainty by validation approach, and parameter uncertainty by sampling methods or surrogate models. The possible sources of uncertainty in L-PBF models including those due to measurement error are identified and captured under the subclass called *LPBFUncertaintySource.* The taxonomy of the uncertainty sources of the top-level entities is depicted in Figure 5.

6.3 Relationships in L-PBF models and uncertainty sources

To capture the interactions between the features of L-PBF phenomena, parameters, and output QoIs at the physical and computational domains, properties that define the relationships are established in the proposed ontology. As described in section 3, the L-PBF models are developed based on assumptions and they do not consider the entire phenomena of the process. Thus, the properties that link these models with their corresponding inputs, outputs, assumptions, and the captured and neglected phenomena are defined in the ontology using *requires*, *predicts*, *assumes*, *considers*, and *neglects*, respectively. Figure 6(a)-(c) shows the relationships in semi-analytical Rosenthal-based thermal model, FEM-based thermal model, and powder-scale thermal-fluid flow model. Similarly, the sources of uncertainty that result in model discrepancy are defined by properties to link different sources with corresponding predictive uncertainties. Those features that cause model form, numerical, parameter, and measurement uncertainties are being captured in the ontology as depicted in Figure 7 and the domains and ranges of properties are clearly defined. For instance, model form uncertainty in (a) powder bed model is caused by assumptions associated with powder bed material distribution and powder size distribution; (b) heat source model is caused by dimensionality of absorbed energy (surface and/or volumetric) and distribution of heat source, and (c) melt pool model is caused by thermal boundary conditions, initial conditions, phase transformation assumptions, and molten metal flow assumptions.

The features that cause variability in some input parameters are captured under parameter uncertainty sources. For example, variability in (a) laser power can be caused by heating of optics, soot on optics and inherent drift in laser delivery system and (b) layer thickness is caused by orientation and positioning errors, vibration in build platform motion, vibration in recoater arm motion, and variation in powder bed density. The main source of numerical uncertainty is discretization errors due to the selection of element size and time steps. Lastly, measurement uncertainty is caused by calibration error, imprecise measurement methods, and variation in measurement results.

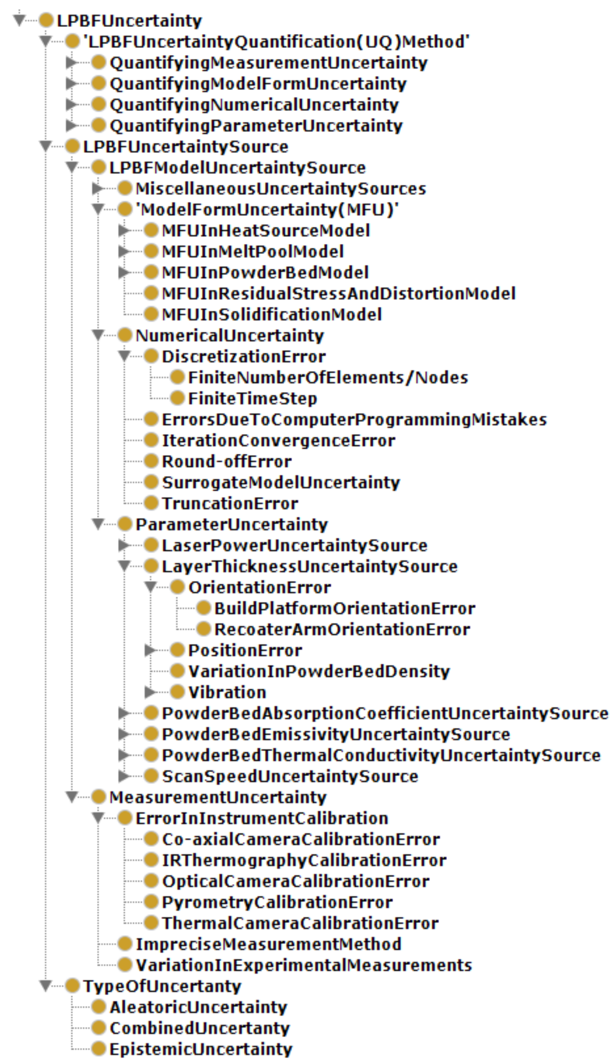

FIGURE 5: HIERARCHICAL REPRESENTATION OF L-PBF UNCERTAINTY SOURCES

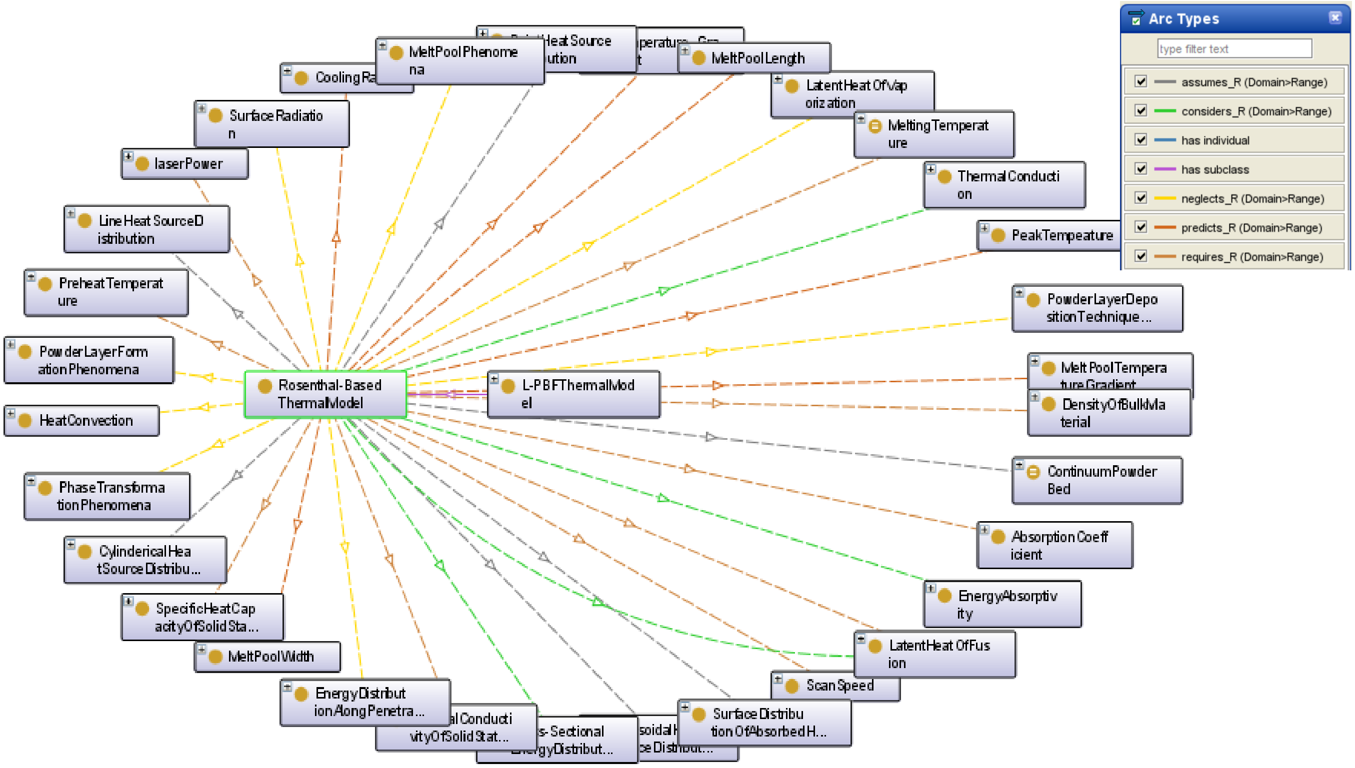

(a) ONTOLOGICAL RELATIONSHIPS IN SEMI-ANALYTICAL ROSENTHAL-BASED THERMAL MODEL

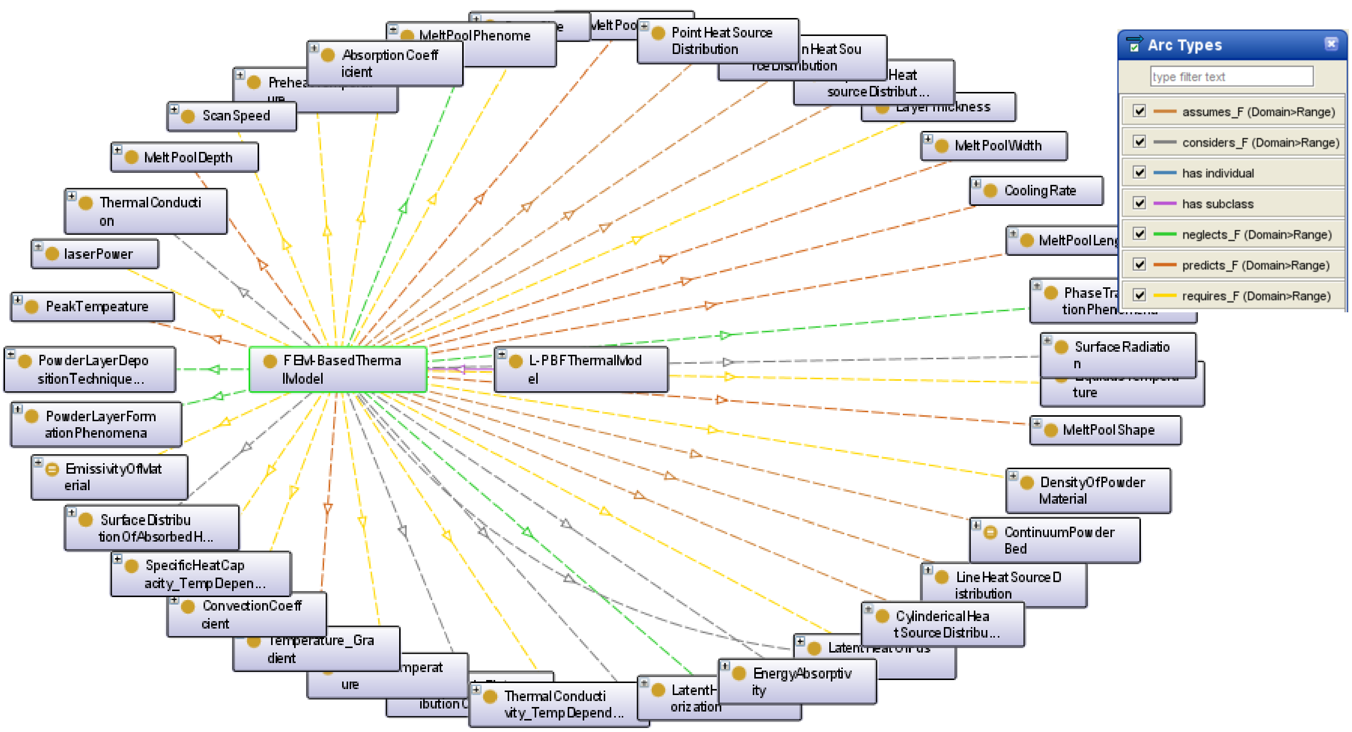

(b) ONTOLOGICAL RELATIONSHIPS IN FEM-BASED THERMAL MODEL

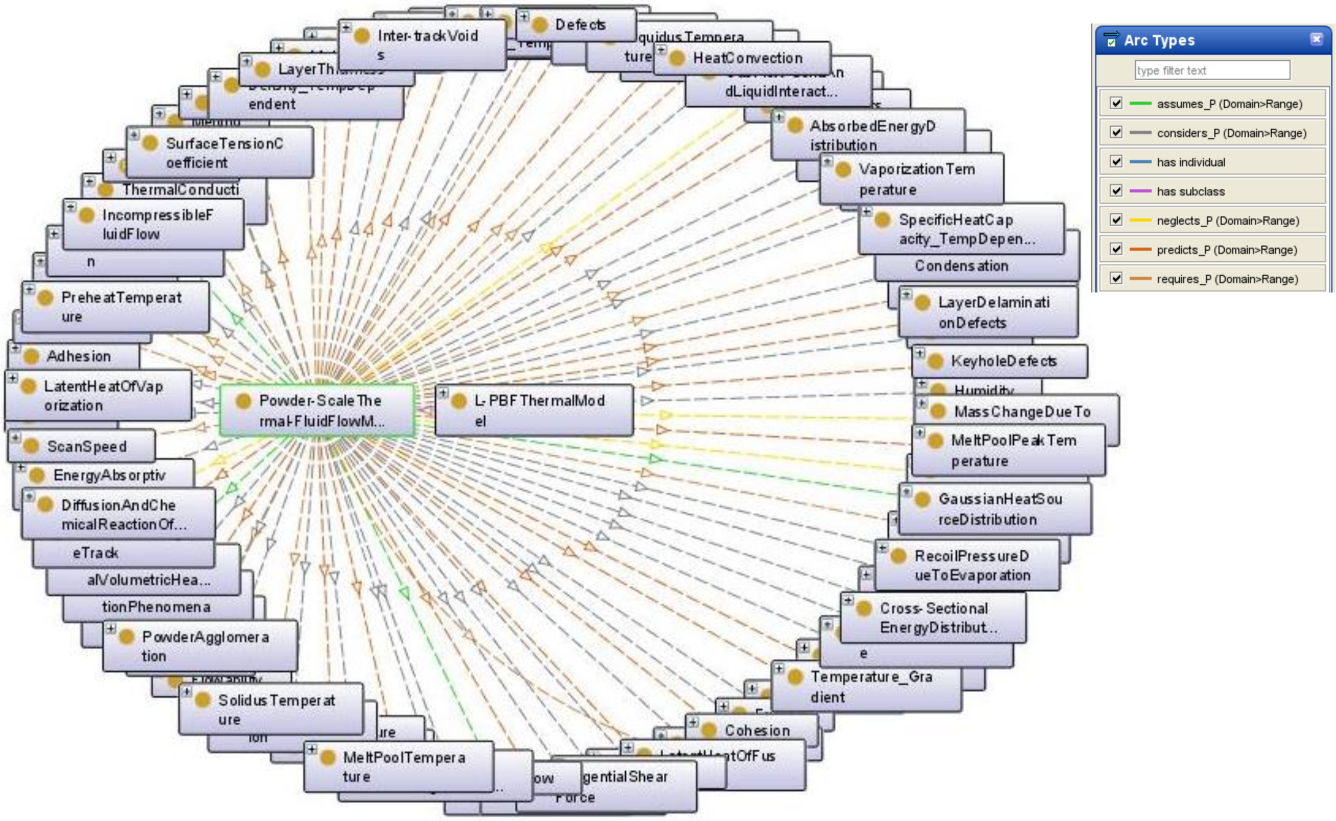

(c) ONTOLOGICAL RELATIONSHIPS IN POWDER-SCALE THERMAL-FLUID FLOW MODEL

FIGURE 6: ONTOLOGICAL RELATIONSHIPS IN L-PBF AM MODELS

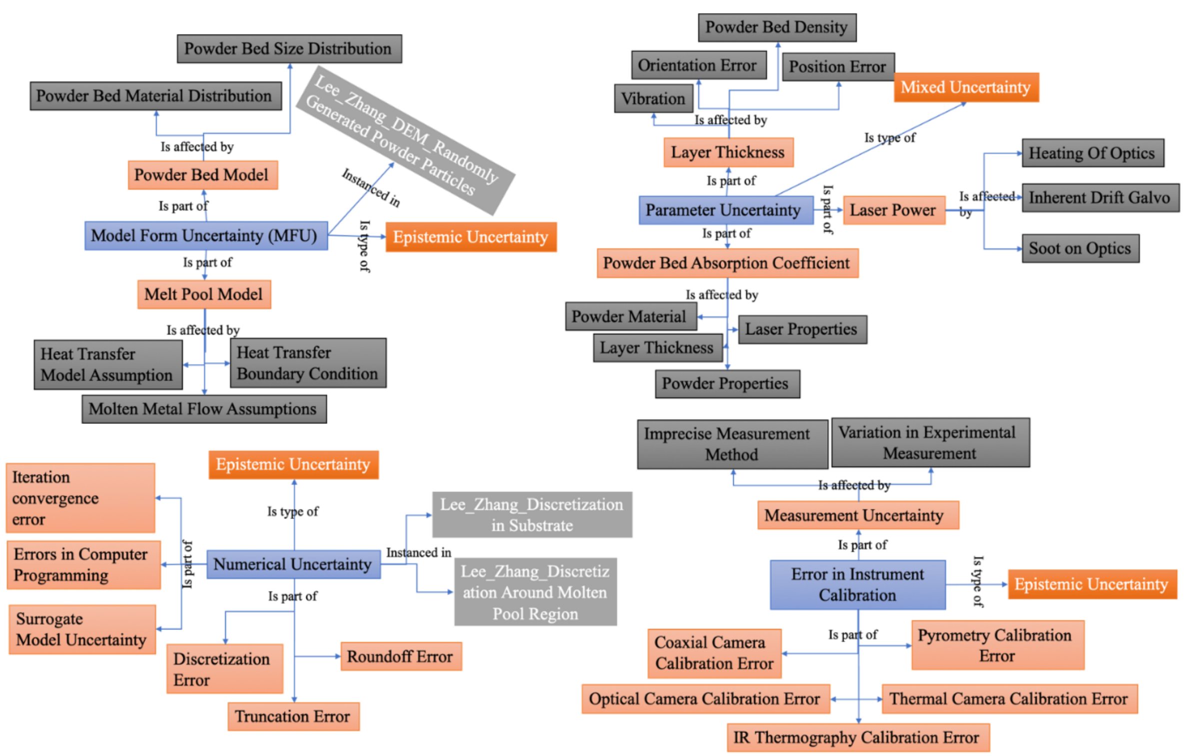

FIGURE 7: SOURCES OF MODEL FORM (TL), NUMERICAL (BL), PARAMETER (TR), AND MEASUREMENT (BR) UNCERTAINTIES

7. CONCLUSIONS

This study explored two major aspects of the L-PBF additive manufacturing process. First, the L-PBF thermal models were characterized focusing on their input parameters, output QoIs, assumptions, and considered and neglected phenomena. These models include Rosenthal-based thermal models, FEM-based thermal models, and powder-scale thermal-fluid flow models. The characterization of the models is necessary to understand the abstraction and formulations of the models and investigate model elements that can be used as a basis for studying the sources of uncertainty which ultimately leads to understanding the predictive accuracy of the models. Then, characterization of sources of uncertainty of the L-PBF models was conducted. These uncertainty sources include model form, numerical, input parameters, and measurement uncertainties. Model form uncertainty is caused by assumptions and simplifications taken during representation of physical phenomena using governing mathematical equations. A validation approach can be used to characterize this source of uncertainty along with model bias by comparing simulation and measurement results. Discretization error associated with element size and time steps is the major cause of numerical uncertainty and a verification approach can be used to characterize and estimate the value of this uncertainty. The presence of natural variability in input variables and imprecise values cause uncertainty in output QoIs. Parameter uncertainty of a model can be determined by using sampling methods either directly on the model, provided that the model is computationally efficient, or through surrogate models that represent the computationally expensive physics-based models. Finally, measurement uncertainty, which is used in model validation, is caused by calibration error, imprecise measurement method, and variation in measurement results, and a standard approach is used to characterize this uncertainty.

This paper also presented ontological representation of the L-PBF models and uncertainty sources. The ontology based on Protégé captures the relevant knowledge associated to process, model, and uncertainty sources. This ontology represents the characterization of the powder-scale thermal-fluid flow models that better imitate the L-PBF process. The class of the L-PBF process mainly captures the physical characteristics, process parameters, and process signatures. Whereas the model ontology class captures model assumptions, formulations, input parameters, outputs, and predictive methods. The L-PBF uncertainty class captures sources of uncertainty, type of uncertainty, and uncertainty quantification methods and approaches. This work can be further extended by incorporating different models ranging from low to high-fidelity to capture more knowledge to assess their predictive capability and compare different models. The topology and mapping of the uncertainty sources presented in this study establish fundamental requirements for measuring model fidelity, and for guiding the selection of a model suitable for its intended purpose.

DISCLAIMER

No approval or endorsement of any commercial product by NIST is intended or implied. Certain commercial equipment, instruments or materials are identified in this report to facilitate better understanding. Such identification does not imply recommendations or endorsement by NIST nor does it imply the materials or equipment identified are necessarily the best available for the purpose.

REFERENCES

[1] Ian, G., David, R., and Brent, S., 2013, *Additive Manufacturing Technologies*, Springer.

[2] Petrovic, V., Vicente Haro Gonzalez, J., Jordá Ferrando, O., Delgado Gordillo, J., Ramón Blasco Puchades, J., and Portolés Griñan, L., 2011, "Additive Layered Manufacturing: Sectors of Industrial Application Shown through Case Studies," Int. J. Prod. Res., **49**(4), pp. 1061–1079.

[3] Prashanth, K. G., Scudino, S., and Eckert, J., 2017, "Defining the Tensile Properties of Al-12Si Parts Produced by Selective Laser Melting," Acta Mater., **126**, pp. 25–35.

[4] Bourell, D. L., Leu, M. C., and Rosen, D. W., 2009, "Roadmap for Additive Manufacturing: Identifying the Future of Freeform Processing," Rapid Prototyp. J., **5**(4), pp. 169–178.

[5] Assouroko, Ibrahim; Lopez, Felipe; Witherell, P., 2016, "A Method for Characterizing Model Fidelity in Laser Powder Bed Fusion Additive Manufacturing," *Proceedings of the ASME 2016 International Mechanical Engineering Congress & Exposition ASME IMECE 2016 November 11-17, 2016, Phoenix, Arizona, USA*, pp. 1–13.

[6] Smith, J., Xiong, W., Yan, W., Lin, S., Cheng, P., Kafka, O. L., Wagner, G. J., Cao, J., and Liu, W. K., 2016, "Linking Process, Structure, Property, and Performance for Metal-Based Additive Manufacturing: Computational Approaches with Experimental Support," Comput. Mech., **57**(4), pp. 583–610.

[7] DebRoy, T., Wei, H. L., Zuback, J. S., Mukherjee, T., Elmer, J. W., Milewski, J. O., Beese, A. M., Wilson-Heid, A., De, A., and Zhang, W., 2018, "Additive Manufacturing of Metallic Components – Process, Structure and Properties," Prog. Mater. Sci., **92**, pp. 112–224.

[8] Moges, T., Ameta, G., and Witherell, P., 2019, "A Review of Model Inaccuracy and Parameter Uncertainty in Laser Powder Bed Fusion Models and Simulations," J. Manuf. Sci. Eng., **141**(4), p. 040801.

[9] Energetics Incorporated, 2013, *Measurement Science Roadmap for Metal-Based Additive Manufacturing*.

[10] Rosenthal, D., 1946, "The Theory of Moving Sources of Heat and Its Application to Metal Treatments," Trans. ASME, pp. 849–866.

[11] King, W. E., Anderson, A. T., Ferencz, R. M., Hodge, N. E., Kamath, C., Khairallah, S. A., and Rubenchik, A. M., 2015, "Laser Powder Bed Fusion Additive Manufacturing of Metals; Physics, Computational, and Materials Challenges," Appl. Phys. Rev., **2**(4), p. 041304.

[12] Gholaminezhad, I., Assimi, H., Jamali, A., and Vajari, D. A., 2016, "Uncertainty Quantification and Robust Modeling of Selective Laser Melting Process Using Stochastic Multi-Objective Approach," Int. J. Adv. Manuf. Technol., **86**(5), pp. 1425–1441.

[13] Adamczak, S., Bochnia, J., and Kaczmarska, B., 2014, "Estimating the Uncertainty of Tensile Strength Measurement for a Photocured Material Produced by Additive Manufacturing," Metrol. Meas. Syst., **21**(3), pp. 553–560.

[14] Hu, Z., and Mahadevan, S., 2017, "Uncertainty Quantification and Management in Additive Manufacturing: Current Status, Needs, and Opportunities," Int. J. Adv. Manuf. Technol., **93**, pp. 2855–2874.

[15] Moges, T., Yan, W., Lin, S., Ameta, G., Fox, J., and Witherell, P.,

2018, "Quantifying Uncertainty in Laser Powder Bed Fusion Additive Manufacturing Models and Simulations," Solid Free. Fabr. Symp., pp. 1913–1928.

[16] Lopez, F., Witherell, P., and Lane, B., 2016, "Identifying Uncertainty in Laser Powder Bed Fusion Additive Manufacturing Models," J. Mech. Des., **138**(November), pp. 1–4.

[17] Moser, D., Beaman, J., Fish, S., and Murthy, J., 2014, "MULTI-LAYER COMPUTATIONAL MODELING OF SELECTIVE LASER SINTERING PROCESSES," Proc. ASME 2014 Int. Mech. Eng. Congr. Expo. IMECE2014, pp. 1–11.

[18] Ma, L., Fong, J., Lane, B., Moylan, S., Filliben, J., Heckert, A., and Levine, L., 2015, "Using Design of Experiments in Finite Element Modeling To Identify Critical Variables for Laser Powder Bed Fusion," Solid Free. Fabr. Symp., pp. 219–228.

[19] Nath, P., Hu, Z., and Mahadevan, S., 2017, "Multi-Level Uncertainty Quantification in Additive Manufacturing," Solid Free. Fabr. 2017 Proc. 28th Annu. Int. S, pp. 922–937.

[20] Kamath, C., 2016, "Data Mining and Statistical Inference in Selective Laser Melting," Int. J. Adv. Manuf. Technol., **86**(5–8), pp. 1659–1677.

[21] Eagar, T. W., and Tsai, N. S., 1983, "Temperature Fields Produced by Traveling Distributed Heat Sources," Weld. J., **62**(12), pp. 346–355.

[22] Verhaeghe, F., Craeghs, T., Heulens, J., and Pandelaers, L., 2009, "A Pragmatic Model for Selective Laser Melting with Evaporation," Acta Mater., **57**(20), pp. 6006–6012.

[23] Tapia, G., King, W. E., Arroyave, R., Johnson, L., Karaman, I., and Elwany, A., 2018, "Uncertainty Propagation Analysis of Computational Models in Laser Powder Bed Fusion Additive Manufacturing Using Polynomial Chaos Expansions," J. Manuf. Sci. Eng., **140**(December).

[24] Tapia, G., Khairallah, S., Matthews, M., King, W. E., and Elwany, A., 2018, "Gaussian Process-Based Surrogate Modeling Framework for Process Planning in Laser Powder-Bed Fusion Additive Manufacturing of 316L Stainless Steel," Int. J. Adv. Manuf. Technol., **94**(9–12), pp. 3591–3603.

[25] Khairallah, S. A., Anderson, A. T., Rubenchik, A., and King, W. E., 2016, "Laser Powder-Bed Fusion Additive Manufacturing: Physics of Complex Melt Flow and Formation Mechanisms of Pores, Spatter, and Denudation Zones," Acta Mater., **108**, pp. 36–45.

[26] Yang, Z., Eddy, D., Krishnamurty, S., Grosse, I., Denno, P., and Lopez, F., 2016, "Investigating Predictive Metamodeling for Additive Manufacturing," Proc. ASME Des. Eng. Tech. Conf., **1**A-**2016**, pp. 1–10.

[27] Yang, Z., Yan, L., Yeung, H., and Krishnamurty, S., 2019, "Investigation of Deep Learning for Real-Time Melt Pool Classification in Additive Manufacturing," *Proceedings of the 2019 IEEE International Conference on Automation Science and Engineering (CASE), Accepted.*, Vancouver, BC, Canada.

[28] Ko, H., Lu, Y., Witherell, P., and Ndiaye, N. Y., 2019, "Machine Learning Based Continuous Knowledge Engineering for Additive Manufacturing," *2019 IEEE 15th International Conference on Automation Science and Engineering (CASE), Accepted.*, Vancouver, BC, Canada.

[29] Razvi, S. S., Feng, S., Narayanan, A., Lee, Y. T., and Witherell, P. "A, 2019, "A Review of Machine Learning Applications in Additive Manufacturing," *Proceedings of the ASME 2019 International Design Engineering Technical Conferences and Computers and Information in Engineering Conference, Accepted*, Anaheim, CA, USA.

[30] Hu, Z., and Mahadevan, S., 2017, "Uncertainty Quantification in Prediction of Material Properties during Additive Manufacturing," Scr. Mater., **135**, pp. 135–140.

[31] Mahmoudi, M., Tapia, G., Karayagiz, K., Franco, B., Ma, J., Arroyave, R., Karaman, I., and Elwany, A., 2018, "Multivariate Calibration and Experimental Validation of a 3D Finite Element Thermal Model for Laser Powder Bed Fusion Metal Additive Manufacturing," Integr. Mater. Manuf. Innov., **7**(3), pp. 116–135.

[32] Ghosh, S., Mahmoudi, M., Johnson, L., Elwany, A., Arroyave, R., and Allaire, D., 2019, "Uncertainty Analysis of Microsegregation during Laser Powder Bed Fusion," Model. Simul. Mater. Sci. Eng., **27**(3), p. 034002.

[33] Zeng, K., Pal, D., and Stucker, B. E., 2012, "A Review of Thermal Analysis Methods in Laser Sintering and Selective Laser Melting," Proc. Solid Free. Fabr. Symp., pp. 796–814.

[34] Schoinochoritis, B., Chantzis, D., and Salonitis, K., 2014, "Simulation of Metallic Powder Bed Additive Manufacturing Processes with the Finite Element Method: A Critical Review," Proc. Inst. Mech. Eng. Part B J. Eng. Manuf., **231**(1), pp. 96–117.

[35] Roberts, I. A., Wang, C. J., Esterlein, R., Stanford, M., and Mynors, D. J., 2009, "A Three-Dimensional Finite Element Analysis of the Temperature Field during Laser Melting of Metal Powders in Additive Layer Manufacturing," Int. J. Mach. Tools Manuf., **49**(12–13), pp. 916–923.

[36] Yan, W., Ge, W., Qian, Y., Lin, S., Zhou, B., Liu, W. K., Lin, F., and Wagner, G. J., 2017, "Multi-Physics Modeling of Single/Multiple-Track Defect Mechanisms in Electron Beam Selective Melting," Acta Mater., **134**, pp. 324–333.

[37] Lee, Y. S., and Zhang, W., 2016, "Modeling of Heat Transfer, Fluid Flow and Solidification Microstructure of Nickel-Base Superalloy Fabricated by Laser Powder Bed Fusion," Addit. Manuf., **12**, pp. 178–188.

[38] Mukherjee, T., Wei, H. L., De, A., and DebRoy, T., 2018, "Heat and Fluid Flow in Additive Manufacturing—Part I: Modeling of Powder Bed Fusion," Comput. Mater. Sci., **150**(February), pp. 304–313.

[39] Yan, W., Lin, S., Kafka, O. L., Lian, Y., Yu, C., Liu, Z., Yan, J., Wolff, S., Wu, H., Ndip-Agbor, E., Mozaffar, M., Ehmann, K., Cao, J., Wagner, G. J., and Liu, W. K., 2018, "Data-Driven Multi-Scale Multi-Physics Models to Derive Process–Structure–Property Relationships for Additive Manufacturing," Comput. Mech., **61**(5), pp. 521–541.

[40] Oberkampf, W. L., and Roy, C. J., 2010, *Verification and Validation in Scientific Computing*, Cambridge University Press, Cambridge.

[41] ASME-V&V-20, 2009, *Standard for Verification and Validation in Computational Fluid Dynamics and Heat Transfer*, American Society of Mechanical Engineers.

[42] Roy, C. J., and Oberkampf, W. L., 2011, "A Comprehensive Framework for Verification, Validation, and Uncertainty Quantification in Scientific Computing," Comput. Methods Appl. Mech. Eng., **200**(25–28), pp. 2131–2144.

[43] Roy, C. J., 2005, "Review of Code and Solution Verification Procedures for Computational Simulation," J. Comput. Phys., **205**(1), pp. 131–156.

[44] PTC 60 / ASME V&V10, 2005, *Guide for Verification and Validation in Computational Solid Mechanics*, The American Society of Mechanical Engineers.

[45] Roache, P., 2001, "Code Verification by the Method of Manufactured Solutions," J. Fluids Eng., **124**(1), pp. 4–10.

[46] Riley, M., and Grandhi, R., 2011, "A Method for the Quantification of Model-Form and Parametric Uncertainties in Physics-Based Simulations," *52nd AIAA/ASME/ASCE/AHS/ASC Structures, Structural Dynamics and Materials Conference*, American

Institute of Aeronautics and Astronautics, Reston, Virigina, pp. 1–10.
[47] Mahesh, M., Lane, B., Donmez, A., Feng, S., Moylan, S., and Fesperman, R., 2015, “Measurement Science Needs for Real-Time Control of Additive Manufacturing Powder Bed Fusion Processes,” NISTIR 8036, Natl. Inst. Stand. Technol., pp. 1–50.
[48] Jcgm, J. C. F. G. I. M., 2008, “Evaluation of Measurement Data — Guide to the Expression of Uncertainty in Measurement,” Int. Organ. Stand. Geneva ISBN, **50**(September), p. 134.
[49] Devesse, W., De Baere, D., and Guillaume, P., 2014, “The Isotherm Migration Method in Spherical Coordinates with a Moving Heat Source,” Int. J. Heat Mass Transf., **75**, pp. 726–735.
[50] Fox, J. C., Lane, B. M., and Yeung, H., 2017, “Measurement of Process Dynamics through Coaxially Aligned High Speed Near-Infrared Imaging in Laser Powder Bed Fusion Additive Manufacturing,” Proc. SPIE 10214, Thermosense Therm. Infrared Appl. XXXIX, **1**(301), p. 1021407.
[51] Kim S, Rosen DW, Witherell P, Ko H., 2019, “A Design for Additive Manufacturing Ontology to Support Manufacturability Analysis,” ASME. *J. Comput. Inf. Sci. Eng*. 19(4), p. 041014-041014-10.
[52] Roh, B., Kumara, S. R. T., Simpson, T. W., and Witherell, P., 2016, “Ontology-Based Laser and Thermal Metamodels for Metal-Based Additive Manufacturing,” Proc. ASME 2016 Int. Des. Eng. Tech. Conf. Comput. Inf. Eng. Conf. IDETC/CIE 2016 August 21-24, 2016, Charlotte, North Carolina, pp. 1–8.